Interplay between strongly localized Eu $4f$ and weakly localized Nb $4d$ electrons in Eu$_3$Nb$_5$O$_{15}$

R. Nakamura,[1] D. Takegami,[1,2] A. Melendez-Sans [ORCID],[2] L. H. Tjeng [ORCID],[2] T. Miyoshino,[1] K. Iwamoto,[3] W. Sekino,[3]
M. Yoshimura [ORCID],[4] K.-D. Tsuei,[4] T. Katsufuji,[3] and T. Mizokawa [ORCID][1]

[1]*Department of Applied Physics, Waseda University, Shinjuku, Tokyo 169-8555, Japan*
[2]*Max Planck Institute for Chemical Physics of Solids, 01187 Dresden, Germany*
[3]*Department of Physics, Waseda University, Shinjuku, Tokyo 169-8555, Japan*
[4]*National Synchrotron Radiation Research Center, 30076 Hsinchu, Taiwan*

We investigated the electronic structure of BaEu$_2$Nb$_5$O$_{15}$ and Eu$_3$Nb$_5$O$_{15}$ by means of hard x-ray photoelectron spectroscopy. The Eu $3d$ core level spectra are primarily dominated by Eu^{2+} signals. The well-screened feature in the Nb $3d$ core level spectra of BaEu$_2$Nb$_5$O$_{15}$ is suppressed in Eu$_3$Nb$_5$O$_{15}$, consistent with the insulating behavior of Eu$_3$Nb$_5$O$_{15}$ due to the atomic disorder and/or the rattling effect of the small Eu ions in the spacious $A2$ site. In the valence band spectra, the Nb $4d$ states at the Fermi level are close to the Eu $4f$ states located around 2 eV below it. This suggests that the degree of localization of the Nb $4d$ electrons can be enhanced through the Eu $4f$–Nb $4d$ hybridization with the atomically and magnetically disordered Eu ions at the $A2$ site.

DOI: 10.1103/PhysRevB.109.165148

I. INTRODUCTION

Among the various conducting oxides, Eu$_{1+x}$O exhibits unique physical properties due to coexistence of the localized Eu $4f$ electrons with $S=7/2$ and the itinerant Eu $5d$ electrons introduced by the excess Eu ions [1–4]. The off-stoichiometry is crucial here, otherwise EuO is insulating. This is also the case for most $3d$ transition-metal oxides, since quite often the d one-electron bandwidth W is smaller than the on-site Coulomb interaction U in the d shell. Whereas the system with d^n configuration becomes a Mott insulator or a band insulator ($n = 0$ or 10), it becomes conducting due to hole or electron doping through off-stoichiometry or chemical substitution [5,6]. In electron-doped d^0 systems such as SrTiO$_{3-\delta}$ and KNbO$_{3-\delta}$ [7,8], the transition-metal d band accommodates low density and high mobility electrons. The low density carriers are somewhat similar to the itinerant Eu $5d$ electrons in EuO. Indeed, the EuTiO$_3$ [9] exhibits unique transport properties when electrons are introduced by La doping [10,11]. In case of $3d$ electrons with $U > W$, correlated d electrons coexist with the highly mobile d electrons and manifest as incoherent spectral features below the Fermi level [7,12–14].

In contrast to the $3d$ systems, $4d$ and $5d$ transition-metal oxides tend to be metallic since W is larger than U [6,15]. Even with the small U/W ratio, several $4d$ systems such as Ca$_{2-x}$Sr$_x$RuO$_4$ [16] and CaCu$_3$Ru$_4$O$_{12}$ [17] exhibit effects of electronic correlation in their Ru $4d$ spectral distribution. Among the various $4d$ systems, Ba$_{3-x}$Sr$_x$Nb$_5$O$_{15}$ with tetragonal tungsten bronze structure [18–21] is unique in that the moderately correlated Nb $4d$ electrons undergo Anderson-type localization due to the ionic radius difference between Ba^{2+} and Sr^{2+} [22,23]. As shown in Fig. 1(a), the tetragonal unit cell includes two $A1$ sites and four $A2$ sites. The compact $A1$ site surrounded by eight NbO$_6$ octahedra has 12 nearest

oxygen atoms and tends to accommodate small ions. The spacious $A2$ site is surrounded by ten NbO$_6$ octahedra (six of them are rather closer to the $A2$ site than the others) and tends to accommodate large ions. In case of Ba$_{3-x}$Sr$_x$Nb$_5$O$_{15}$, the system is a good metal with a partially filled Nb $4d$ band for $0 \leqslant x \leqslant 1$ where the small Sr ions selectively occupy the compact $A1$ site. The small Sr ions enter the spacious $A2$ site for $x \geqslant 1.5$, introducing substantial lattice disorder, and consequently the system becomes semiconducting or even insulating [22,23]. The electronic correlation effect manifests as incoherent spectral features of Nb $4d$ which was probed by hard x-ray photoemission spectroscopy (HAXPES) on Ba$_{3-x}$Sr$_x$Nb$_5$O$_{15}$ [25].

In Ba$_{3-x}$Sr$_x$Nb$_5$O$_{15}$, the transport properties of the Nb-O network are controlled by the atomic disorder introduced in the A sites [22,23,26,27]. In this context, it would be even more interesting if the transport properties can be controlled through magnetic ions introduced in the A sites. Indeed, Iwamoto *et al.* introduced Eu ions in the $A1$ and $A2$ sites and discovered interesting interplay between the Eu^{2+} spins and the conducting electrons [28]. While Eu$_3$Nb$_5$O$_{15}$ is insulating, BaEu$_2$Nb$_5$O$_{15}$ is a bad metal and exhibits large negative magnetoresistance at low temperatures [28,29]. As shown in Fig. 1(b), Eu^{2+} takes the $4f^7$ configuration with $S = 7/2$. In Eu$_3$Nb$_5$O$_{15}$, the small Eu^{2+} ions occupy both of the compact $A1$ and spacious $A2$ sites which may have different magnetic interaction with the Nb $4d$ electrons. When the small Eu^{2+} ions are partially replaced by the large Ba^{2+} ions, Ba^{2+} are expected to occupy the spacious $A2$ site as illustrated in Fig. 1(a). The interplay between the magnetic and structural coupling between the $A1/A2$ sites and the Nb site is highly interesting. In addition, since the distance between the Eu ions and the Nb ions is relatively small in the present system, the charge transferred state with Eu^{3+} ($4f^6$) and Nb^{4+} ($4d^1$) may play important roles through strong hybridization between the Eu $4f$ and Nb $4d$ orbitals. In this context, it is interesting to study
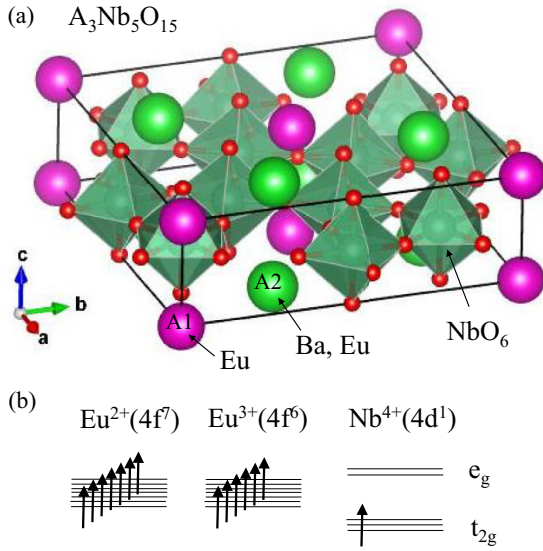
FIG. 1. (a) Crystal structure of $Eu_3Nb_5O_{15}$ illustrated by VESTA [24]. (b) Electronic configurations of Eu^{2+} ($4f^7$), Eu^{3+} ($4f^6$), and Nb^{4+} ($4d^1$).

evolution of Eu $4f$ and Nb $4d$ states in $Ba_xEu_{3-x}Nb_5O_{15}$ by means of HAXPES.

In the present paper, we focus on the fundamental electronic structure of $Eu_3Nb_5O_{15}$ and $BaEu_2Nb_5O_{15}$ with the Ba ions only at the spacious $A2$ site and with Eu ions at both of the compact $A1$ and spacious $A2$ sites. We have performed HAXPES for their single crystals in order to reveal the site dependent electronic state of Eu and the interplay between the Eu $4f$ and Nb $4d$ electrons.

II. EXPERIMENT

The single crystals were grown by floating zone method as reported elsewhere [28]. HAXPES measurements were performed at the Max-Planck-NSRRC HAXPES endstation [30], Taiwan undulator beam line BL12XU of SPring-8 with 6.5-keV photon energy. The probing depth determined by the inelastic mean free path of the photoelectrons (with the kinetic energy of 5.5–6.5 keV) is estimated to be about 4–5 nm in the universal curve [31] and is about 10 nm for various inorganic compounds in the recent calculations [32]. The inelastic mean free path is at least ten times larger than the lattice constant (about 4 Å) along the c axis of $Eu_3Nb_5O_{15}$ and $BaEu_2Nb_5O_{15}$. Therefore, the ratio of signals from the surface layer in the total signals is estimated to be smaller than $1 - e^{1/10}$ (about 10%). The x-ray incidence angle was $15°$ with respect to the sample surface, and the photoelectron detection angle was $15°$ off from the surface normal of the sample and parallel to the E vector of the x ray. The single crystals were fractured under ultrahigh vacuum of 10^{-6} Pa at 300 K in order to obtain clean sample surfaces. The measurements were conducted at 300 K. The total energy resolution was about 300 meV.

III. RESULTS AND DISCUSSION

Figure 2(a) shows survey scans for $BaEu_2Nb_5O_{15}$ and $Eu_3Nb_5O_{15}$. The intensities of Eu $3d$, Ba $3d$, O $1s$, and Nb $3d$
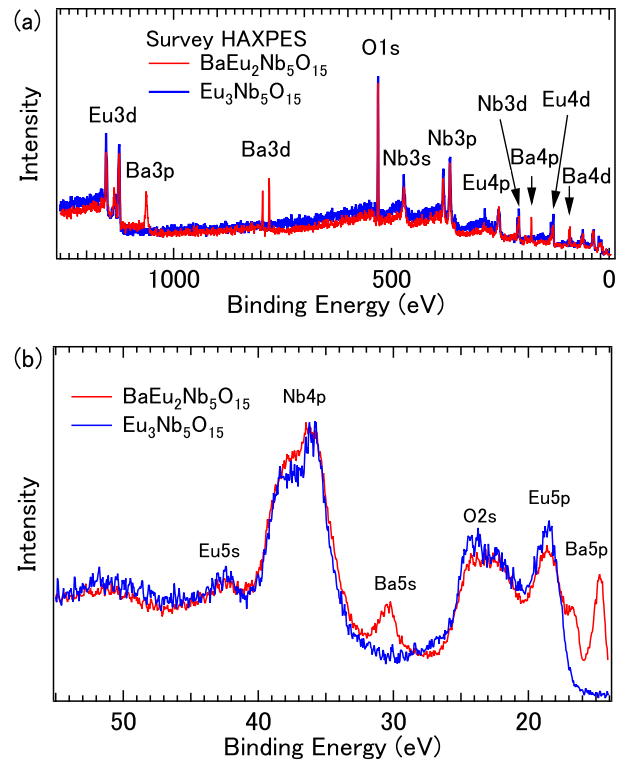
FIG. 2. (a) Survey scans of $BaEu_2Nb_5O_{15}$ and $Eu_3Nb_5O_{15}$. (b) Shallow core levels of $BaEu_2Nb_5O_{15}$ and $Eu_3Nb_5O_{15}$.

core levels are roughly consistent with the compositions. The HAXPES spectra of shallow core levels including Nb $4p$, Eu $5s$, Ba $5s$, Eu $5p$, Ba $5p$, and O $2s$ are shown in Fig. 2(b). The spin-orbit splitting between $p_{3/2}$ and $p_{1/2}$ branches is observed for Nb $4p$, Eu $5p$, and Ba $5p$.

O $1s$ HAXPES spectra for $BaEu_2Nb_5O_{15}$ and $Eu_3Nb_5O_{15}$ are displayed in Fig. 3(a). In going from $BaEu_2Nb_5O_{15}$ to $Eu_3Nb_5O_{15}$, the O $1s$ binding energy increases by ≈ 0.2 eV. This is consistent with the O $1s$ binding energy increase by Sr substitution for Ba [25]. In addition, the O $1s$ peak is almost symmetric in $Eu_3Nb_5O_{15}$ while $BaEu_2Nb_5O_{15}$ exhibits the asymmetric O $1s$ peak. The reduction of the binding energy and of the shape asymmetry can be assigned to a decrease of the screening effect. Since the Nb $4d$ electrons are fewer or more localized in $Eu_3Nb_5O_{15}$ than in $BaEu_2Nb_5O_{15}$, the Doniach-Šunjić effect by conduction electrons is smaller in $Eu_3Nb_5O_{15}$. Figure 3(b) shows Nb $3d$ and Ba $4p_{1/2}$ HAXPES spectra. The broad contribution around 204 eV is due to energy loss peak for Ba $4p_{3/2}$ in $BaEu_2Nb_5O_{15}$. In addition to the main Nb $3d_{5/2}$ and Nb $3d_{3/2}$ peaks (poorly screened feature), shoulders are observed on the lower binding energy side (corresponding to well screened feature). In $Eu_3Nb_5O_{15}$, the suppression of the well-screened feature of Nb $3d$ is consistent with the symmetric O $1s$ peak. These observations are consistent with the transport properties [28] and suggest that the Nb $4d$ electrons are depleted or are localized in $Eu_3Nb_5O_{15}$.

Figure 4 shows Eu $3d$ core level spectra of $BaEu_2Nb_5O_{15}$ and $Eu_3Nb_5O_{15}$. The Eu $3d$ core level spectra are dominated by Eu^{2+} signals for $3d_{5/2}$ and $3d_{3/2}$ around 1125 and 1156 eV, respectively. The $3d_{5/2}$ and $3d_{3/2}$ main peaks
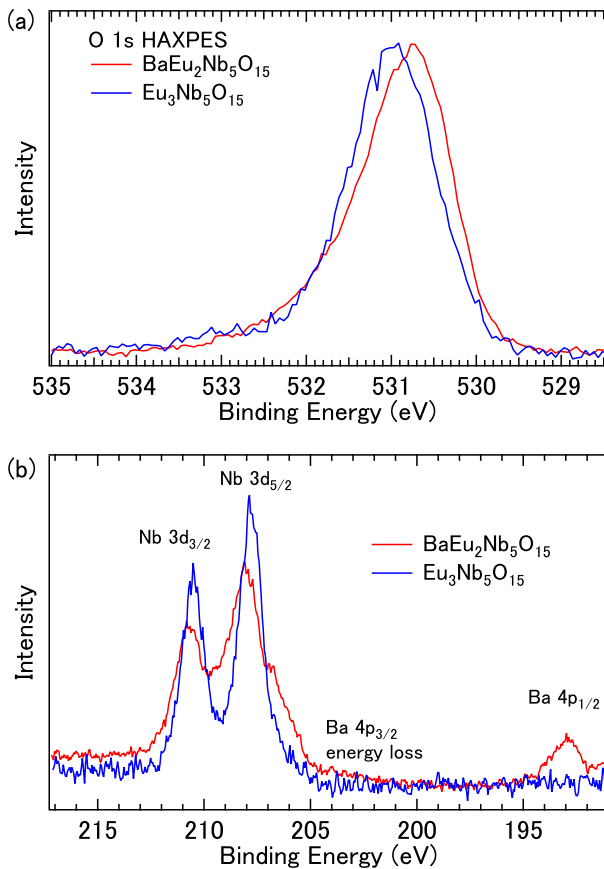
FIG. 3. (a) O $1s$ core level spectra of $BaEu_2Nb_5O_{15}$ and $Eu_3Nb_5O_{15}$. (b) Nb $3d$ and Ba $4p_{1/2}$ core level spectra of $BaEu_2Nb_5O_{15}$ and $Eu_3Nb_5O_{15}$.

are accompanied by the satellite peaks around 1134 and 1165 eV in addition to the exchange splitting ($\approx$8 eV for $3d_{5/2}$ and $\approx$6 eV for $3d_{3/2}$ [33]), respectively. The satellite peak of $3d_{5/2}$ is affected by a coincidental overlap with the Ba $3p_{1/2}$ peak in $BaEu_2Nb_5O_{15}$. The satellite peaks are derived
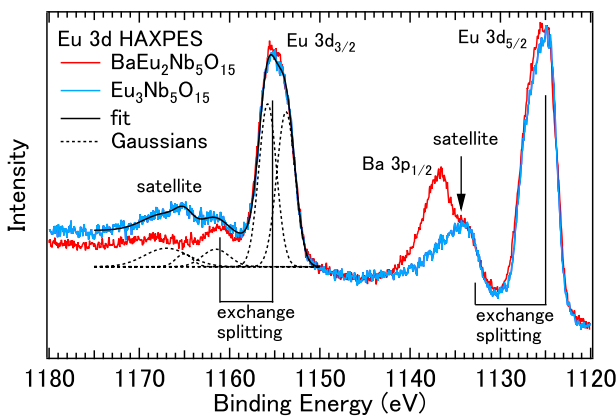
FIG. 4. Eu $3d$ core level spectra of $BaEu_2Nb_5O_{15}$ and $Eu_3Nb_5O_{15}$. The black solid curve represents a fit with five Gaussian functions and a Shirley background to the Eu $3d_{3/2}$ branch of $Eu_3Nb_5O_{15}$. The five Gaussian components are plotted by the broken curves.

from the charge transfer effect (Kotani-Toyozawa effect) in the final state [33–35] or the Eu^{2+}/Eu^{3+} mixed valence in the ground state [36]. The satellite peak around 1165 eV is clearly observed in $Eu_3Nb_5O_{15}$ while it is suppressed in $BaEu_2Nb_5O_{15}$.

In the scenario of the charge transfer, the Nb $4d$ or O $2p$ electron is transferred to the Eu $4f$ orbitals in the final state since the energy of the Eu $4f$ states is lowered by the Eu $3d$ core hole potential. The final states of the main and satellite peaks are respectively given by $\cos\theta|cf^7\rangle + \sin\theta|cf^8L\rangle$ and $\sin\theta|cf^7\rangle - \cos\theta|cf^8L\rangle$, where c and L denote an Eu $3d$ core hole and a Nb $4d$ or O $2p$ hole, respectively. The transition probabilities from the f^7 ground state to the main and satellite final states are proportional to $\cos^2\theta$ and $\sin^2\theta$, respectively. The intensity of the satellite peak is expected to increase with the nondiagonal term between $|cf^7\rangle$ and $|cf^8L\rangle$ through the Eu $4f$–Nb $4d$/O $2p$ transfer integrals. In the scenario of the mixed valence, the ground state is given by $\cos\phi|f^7\rangle + \sin\phi|f^6v\rangle$, where v denotes a Nb $4d$ electron. The final states of the main and satellite peaks are respectively given by $\cos\phi'|cf^7\rangle + \sin\phi'|cf^6v\rangle$ and $\sin\phi'|cf^7\rangle - \cos\phi'|cf^6v\rangle$. The transition probabilities from the ground state to the main and satellite final states are proportional to $|\cos\phi\cos\phi' + \sin\phi\sin\phi'|^2$ and $|\cos\phi\sin\phi' - \sin\phi\cos\phi'|^2$, respectively. As clearly seen in the $3d_{3/2}$ branch, the intensity of the satellite relative to that of the main peak is much higher in $Eu_3Nb_5O_{15}$ than in $BaEu_2Nb_5O_{15}$. In $BaEu_2Nb_5O_{15}$, the compact $A1$ sites are already fully occupied by the relatively small Eu ions in a selective way. In going from $BaEu_2Nb_5O_{15}$ to $Eu_3Nb_5O_{15}$, the Ba ions in the spacious $A2$ sites are replaced by the small Eu ions. Since the Eu $4f$–Nb $4d$/O $2p$ hybridization is expected to be similar between $BaEu_2Nb_5O_{15}$ and $Eu_3Nb_5O_{15}$, the charge transfer effect cannot explain the increase of the satellite peak in $Eu_3Nb_5O_{15}$. As for the mixed valence effect, although the magnetic moment is very close to the atomic value of Eu^{2+} ($4f^7$) [28], a small amount of Eu^{3+} ($4f^6v$) can be mixed into the ground state through the Eu $4f$–Nb $4d$ hybridization or the oxygen off-stoichiometry. Since the Nb $4d$ orbitals are mostly unoccupied (the average valence of Nb is close to +4.8 as expected from the composition and confirmed by the thermogravimetric analysis [29]), the transfer integrals between $4f^7$ and $4f^6v$ for the mixed valence state are much larger than those between $4f^7$ and $4f^8L$ for the charge transfer effect. Based on the arguments, the Eu $3d$ satellite peaks in $Eu_3Nb_5O_{15}$ can be assigned to the mixed valence state rather than the charge transfer effect in the final states. The area ratio between the main and satellite peaks is estimated to be about 0.11 by the curve fit with five Gaussian functions indicated by the black solid curve in Fig. 4. Assuming that the nondiagonal term (Eu $4f$–Nb $4d$ transfer integrals) is much smaller than the energy difference of the diagonal terms $\approx$9 eV (namely $\phi' \approx 0$), this value corresponds to the population of Eu^{3+} per site. Here, one cannot exclude the possibility that the Eu^{3+} component (about 10% spectral weight of the Eu $3d_{3/2}$) is derived from the surface. However, such surface effect is expected to be common between $Eu_3Nb_5O_{15}$ and $BaEu_2Nb_5O_{15}$. Since the Eu^{3+} component is negligibly small in $BaEu_2Nb_5O_{15}$, the Eu^{3+} signal in $Eu_3Nb_5O_{15}$ can be assigned to the difference of the bulk electronic structure rather than the surface effect.
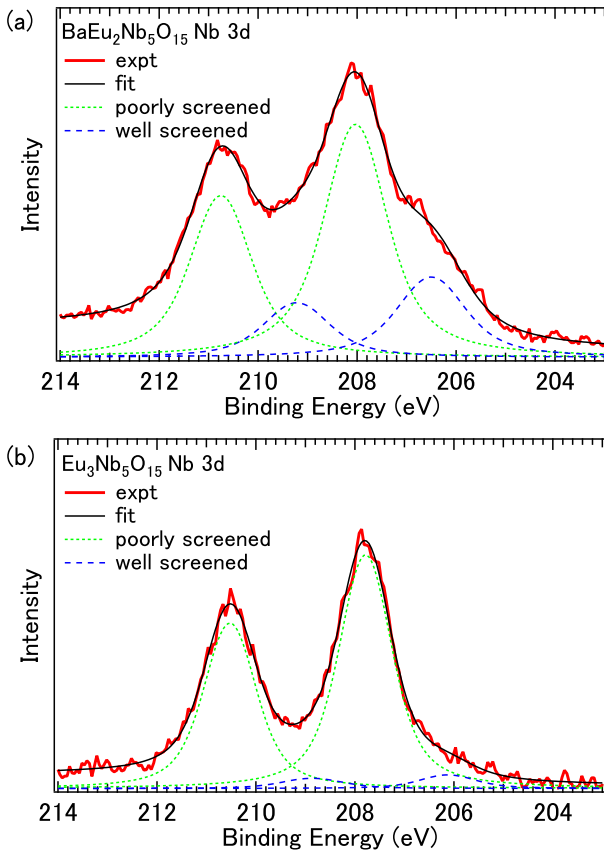
FIG. 5. Voigt function fitting to Nb $3d$ core level spectra of (a) $BaEu_2Nb_5O_{15}$ and (b) $Eu_3Nb_5O_{15}$.

FIG. 6. (a) Valence band spectra of $BaEu_2Nb_5O_{15}$ and $Eu_3Nb_5O_{15}$ compared with that of $BaSr_2Nb_5O_{15}$ reported in [25]. The spectral weight of the O $2p$ band is mainly derived from the Ba $5p$ and Eu $5p$ components mixed into the O $2p$ states. (b) Zoom near the Fermi level for $BaEu_2Nb_5O_{15}$ and $Eu_3Nb_5O_{15}$ compared with that of $BaSr_2Nb_5O_{15}$. The solid curve represents a fit with two Gaussian functions. The Gaussian functions and a Shirley background are indicated by broken and dashed curves, respectively.

The well-screened and poorly screened features in the Nb $3d$ spectra are observed in various $4d$ transition-metal oxides with moderate correlation effect such as $Ca_{2-x}Sr_xRuO_4$ [37–40]. In Fig. 5, the intensity ratio between the well-screened and poorly screened peaks in the Nb $3d$ core level spectra is estimated by fitting the spectra to four Voigt functions. The area of the well-screened feature relative to the total area is estimated to be $0.37/(1+0.37) \approx 0.27$ for $BaEu_2Nb_5O_{15}$ which is close to the value for $BaSr_2Nb_5O_{15}$ reported by Yasuda *et al.* [25]. This indicates that the degree of the Nb $4d$ electron localization is similar between $BaEu_2Nb_5O_{15}$ and $BaSr_2Nb_5O_{15}$. In $BaEu_2Nb_5O_{15}$, the Nb $4d$ electrons are still itinerant although they are already affected by the static lattice disorder and/or the dynamic rattling effect introduced by the small ions (Eu or Sr) in the spacious $A2$ site. The well-screened feature is almost suppressed in $Eu_3Nb_5O_{15}$. Indeed, the area of the well-screened feature relative to the total area is estimated to be about 0.06 by the fitting to the Voigt functions. Assuming that the number of Nb $4d$ electrons is not affected by the substitution of Eu^{2+} for Ba^{2+}, the suppression of the screened feature can be assigned to localization of the $4d$ electrons. This speculation is consistent with the fact that the $A2$ site is fully occupied by the Eu ions in $Eu_3Nb_5O_{15}$, and the disorder effect and/or the rattling effect is stronger than that in $BaEu_2Nb_5O_{15}$.

Figure 6(a) shows the valence band HAXPES spectra. Both in $BaEu_2Nb_5O_{15}$ and $Eu_3Nb_5O_{15}$, the O $2p$ band is observed in the energy range from 4 to 10 eV similar to $BaSr_2Nb_5O_{15}$ [25]. The photoionization cross section of O $2p$ is negligibly small compared to those of Nb $4d$, Ba $5p$, and Eu $5p/4f/5d$ [41,42]. The spectral weight of the O $2p$ band is mainly derived from the Ba $5p$ and Eu $5p$ components mixed into the O $2p$ band. Although the amounts of the Ba $5p$ and Eu $5p$ components are minute, these $5p$ states have two orders of magnitude larger cross section so that they contribute significantly to the HAXPES valence band spectra [43]. The Eu $4f$ peak is located around 2 eV below the Fermi level. Compared with the intense Eu $4f$ peak, the Nb $4d$ spectral weight near the Fermi level is rather small. Since the photoionization cross section of Eu $4f$ is comparable to that of Nb $4d$ [41,42], the weak $4d$ band is consistent with the relatively small electron number (about one $4d$ electron per formula unit with five Nb sites) compared to the 21 $4f$ electrons per formula unit.

Figure 6(b) shows the HAXPES spectra near the Fermi level. The Eu $4f$ peak energy ≈ 2 eV is very similar to that of EuO. Interestingly, in $BaEu_2Nb_5O_{15}$, the Eu $4f$ peak has a shoulder on the lower binding energy side. It is possible to assign the lower and higher binding energy components to the $A1$ and $A2$ sites, respectively. Indeed, the Eu $4f$ peak can be

fitted by two Gaussian functions as shown in Fig. 6(b). The area ratio of the Gaussian for $A2$ to that for $A1$ is about 1.3. This is consistent with the previous observation in $Ba_3Nb_5O_{15}$ in which the Ba 5p binding energy is lower in the $A1$ site than in the $A2$ site. In going from $BaEu_2Nb_5O_{15}$ to $Eu_3Nb_5O_{15}$, the Ba ions at the $A2$ site are replaced by the Eu ions and the intensity of the higher binding energy component at $\approx$2 eV is almost doubled. The Nb 4d spectral weight is distributed from the Fermi level to $\approx$0.5 eV and the onset of the Eu 4f peak is located around 0.6 eV both in $BaEu_2Nb_5O_{15}$ and $Eu_3Nb_5O_{15}$. The energy difference between the O 2p band and the Nb 4d band is not sensitive to the substitution of A-site ions. Since the energy range of the O 2p band of $Eu_3Nb_5O_{15}$ is the same as that of $BaEu_2Nb_5O_{15}$, one can speculate that the number of 4d electrons of $Eu_3Nb_5O_{15}$ is similar to $BaEu_2Nb_5O_{15}$. The finite Nb 4d spectral weight at the Fermi level excludes band gap opening as an origin of the insulating behavior of $Eu_3Nb_5O_{15}$. Similar to $Ba_{3-x}Sr_xNb_5O_{15}$, it can be assigned to the Anderson localization due to the static disorder and/or the dynamic rattling effect of the small Eu ions in the spacious $A2$ site. Since the Nb 4d states at the Fermi level are energetically close to the Eu 4f states, the degree of localization of the Nb 4d electrons can be enhanced through the Eu 4f–Nb 4d hybridization with the atomically and magnetically disordered Eu ions at the $A2$ site. However, the direct hybridization between the Eu 4f and Nb 4d bands should be confirmed by angle-resolved photoemission spectroscopy as previously demonstrated for $EuNi_2P_2$ [44]. $Eu_3Nb_5O_{15}$ is a very unique magnetic system in which the atomically localized Eu 4f electrons hybridize with the Nb 4d electrons under the Anderson localization to harbor the large negative magnetoresistance [28].

IV. CONCLUSION

In conclusion, we have investigated the electronic structure of $BaEu_2Nb_5O_{15}$ and $Eu_3Nb_5O_{15}$ by means of hard x-ray photoemission spectroscopy. In $Eu_3Nb_5O_{15}$, the Eu 3d core level spectra are dominated by Eu^{2+} signals with the satellites. The satellite structure of Eu 3d gains intensity in $Eu_3Nb_5O_{15}$ suggesting a minor but non-negligible Eu^{3+} contribution. The well-screened feature in the Nb 3d core level spectrum of $BaEu_2Nb_5O_{15}$ resembles that of $BaSr_2Nb_5O_{15}$, indicating that the Nb 4d electrons are still itinerant under the lattice disorder and/or the rattling effect introduced by the small Eu/Sr ions in the spacious $A2$ site. The well-screened feature is almost suppressed in $Eu_3Nb_5O_{15}$ due to the Anderson localization of the Nb 4d electrons. In the valence band spectra, the Nb 4d states at the Fermi level are close to the Eu 4f states, suggesting that the degree of Anderson localization of the Nb 4d electrons can be enhanced through the Eu 4f–Nb 4d hybridization with the atomically disordered Eu ions at the $A2$ site. $Eu_3Nb_5O_{15}$ is a unique magnetic system in which the strongly localized Eu 4f electrons interact with the weakly localized Nb 4d electrons.

[1] G. Petrich, S. von Molnár, and T. Penney, Phys. Rev. Lett. **26**, 885 (1971).

[2] Y. Shapira, S. Foner, and T. B. Reed, Phys. Rev. B **8**, 2299 (1973).

[3] P. G. Steeneken, L. H. Tjeng, I. Elfimov, G. A. Sawatzky, G. Ghiringhelli, N. B. Brookes, and D.-J. Huang, Phys. Rev. Lett. **88**, 047201 (2002).

[4] D. E. Shai, A. J. Melville, J. W. Harter, E. J. Monkman, D. W. Shen, A. Schmehl, D. G. Schlom, and K. M. Shen, Phys. Rev. Lett. **108**, 267003 (2012).

[5] M. Imada, A. Fujimori, and Y. Tokura, Rev. Mod. Phys. **70**, 1039 (1998).

[6] D. I. Khomskii, *Transition Metal Compounds*, (Cambridge University, New York, 2014).

[7] A. Chikina, F. Lechermann, M.-A. Husanu, M. Caputo, C. Cancellieri, X. Wang, T. Schmitt, M. Radovic, and V. N. Strocov, ACS Nano **12**, 7927 (2018).

[8] G. Li, H. Huang, S. Peng, Y. Xiong, Y. Xiao, S. Yan, Y. Cao, M. Tang, and Z. Li, RSC Adv. **9**, 35499 (2019).

[9] T. Katsufuji and H. Takagi, Phys. Rev. B **64**, 054415 (2001).

[10] T. Katsufuji and Y. Tokura, Phys. Rev. B **60**, R15021(R) (1999).

[11] K. S. Takahashi, H. Ishizuka, T. Murata, Q. Y. Wang, Y. Tokura, N. Nagaosa, and M. Kawasaki, Sci. Adv. **4**, eaar7880 (2018).

[12] M. Takizawa, H. Wadati, K. Tanaka, M. Hashimoto, T. Yoshida, A. Fujimori, A. Chikamatsu, H. Kumigashira, M. Oshima, K. Shibuya, T. Mihara, T. Ohnishi, M. Lippmaa, M. Kawasaki, H. Koinuma, S. Okamoto, and A. J. Millis, Phys. Rev. Lett. **97**, 057601 (2006).

[13] Y. Ishida, R. Eguchi, M. Matsunami, K. Horiba, M. Taguchi, A. Chainani, Y. Senba, H. Ohashi, H. Ohta, and S. Shin, Phys. Rev. Lett. **100**, 056401 (2008).

[14] X. Hao, Z. Wang, M. Schmid, U. Diebold, and C. Franchini, Phys. Rev. B **91**, 085204 (2015).

[15] T. Mizokawa, J. Electron Spectrosc. Relat. Phenom. **208**, 78 (2016).

[16] M. Kim, J. Kwon, C. H. Kim, Y. Kim, D. Chung, H. Ryu, J. Jung, B. S. Kim, D. Song, J. D. Denlinger, M. Han, Y. Yoshida, T. Mizokawa, W. Kyung, and C. Kim, npj Quantum Mater. **7**, 59 (2022).

[17] D. Takegami, C.-Y. Kuo, K. Kasebayashi, J.-G. Kim, C. F. Chang, C. E. Liu, C. N. Wu, D. Kasinathan, S. G. Altendorf, K. Hoefer, F. Meneghin, A. Marino, Y. F. Liao, K. D. Tsuei, C. T. Chen, K.-T. Ko, A. Günther, S. G. Ebbinghaus, J. W. Seo, D. H. Lee *et al.*, Phys. Rev. X **12**, 011017 (2022).

[18] P. B. Jamieson, S. C. Abrahams, and J. L. Bernstein, J. Chem. Phys. **48**, 5048 (1968).

[19] B. Hessen, S. A. Sunshine, T. Siegrist, A. T. Fiory, and J. V. Waszczak, Chem. Mater. **3**, 528 (1991).

[20] B. Hessen, S. A. Sunshine, T. Siegrist, and R. Jimenez, Mater. Res. Bull. **26**, 85 (1991).

[21] Y. K. Hwang and Y.-U. Kwon, Mater. Res. Bull. **32**, 1495 (1997).

[22] T. Kolodiazhnyi, H. Sakurai, M. Isobe, Y. Matsushita, S. Forbes, Y. Mozharivskyj, T. J. S. Munsie, G. M. Luke, M. Gurak, and D. R. Clarke, Phys. Rev. B **92**, 214508 (2015).

[23] Y. Kondoh, R. Takei, T. Okuda, K. Ueno, Y. Katayama, T. Saiki, W. Sekino, T. Kajita, and T. Katsufuji, Phys. Rev. B **104**, 125128 (2021).

[24] K. Momma and F. Izumi, J. Appl. Crystallogr. **44**, 1272 (2011).

[25] T. Yasuda, Y. Kondo, T. Kajita, K. Murota, D. Ootsuki, Y. Takagi, A. Yasui, N. L. Saini, T. Katsufuji, and T. Mizokawa, Phys. Rev. B **102**, 205133 (2020).

[26] T. Kolodiazhnyi, H. Sakurai, O. Vasylkiv, H. Borodianska, and Y. Mozharivskyj, Appl. Phys. Lett. **104**, 111903 (2014).

[27] G. M. Pugliese, F. G. Capone, L. Tortora, F. Stramaglia, L. Simonelli, C. Marini, Y. Kondoh, T. Kajita, T. Katsufuji, T. Mizokawa, and N. L. Saini, Mater. **15**, 4402 (2022).

[28] K. Iwamoto, W. Sekino, S. Ito, Y. Katayama, K. Ueno, and T. Katsufuji, J. Phys. Soc. Jpn. **91**, 033702 (2022).

[29] W. Sekino, R. Takei, S. Ito, H. Takei, K. Iwamoto, Y. Katayama, K. Ueno, H. Kuwahara, and T. Katsufuji, Phys. Rev. Mater. **7**, 124404 (2023).

[30] J. Weinen, T. C. Koethe, C. F. Chang, S. Agrestini, D. Kasinathan, Y. F. Liao, H. Fujiwara, C. Schler-Langeheine, F. Strigari, T. Haupricht, G. Panaccione, F. Offi, G. Monaco, S. Huotari, K.-D. Tsuei, and L. H. Tjeng, J. Electron Spectrosc. Relat. Phenom. **198**, 6 (2015).

[31] M. P. Seah and W. A. Dench, Surf. Interface Anal. **1**, 2 (1979).

[32] H. Shinotsuka, S. Tanuma, C. J. Powell, and D. R. Penn, Surf. Interface Anal. **51**, 427 (2019).

[33] E.-J. Cho, S.-J. Oh, S. Imada, S. Suga, T. Suzuki, and T. Kasuya, Phys. Rev. B **51**, 10146 (1995).

[34] A. Kotani and H. Ogasawara, J. Electron Spectrosc. Relat. Phenom. **60**, 257 (1992).

[35] C. Caspers, M. Müller, A. X. Gray, A. M. Kaiser, A. Gloskovskii, C. S. Fadley, W. Drube, and C. M. Schneider, Phys. Rev. B **84**, 205217 (2011).

[36] M. Müller, P. Lömker, P. Rosenberger, M. H. Hamed, D. N. Mueller, R. A. Heinen, T. Szyjka, and L. Baumgarten, J. Vacuum Sci. Technology A **40**, 013215 (2022).

[37] H.-D. Kim, H.-J. Noh, K. H. Kim, and S.-J. Oh, Phys. B: Condens. Matter **359-361**, 1267 (2005).

[38] Z. V. Pchelkina, I. A. Nekrasov, Th. Pruschke, A. Sekiyama, S. Suga, V. I. Anisimov, and D. Vollhardt, Phys. Rev. B **75**, 035122 (2007).

[39] G. Zhang and E. Pavarini, Phys. Rev. B **95**, 075145 (2017).

[40] A. Chikamatsu, Y. Kurauchi, K. Kawahara, T. Onozuka, M. Minohara, H. Kumigashira, E. Ikenaga, and T. Hasegawa, Phys. Rev. B **97**, 235101 (2018).

[41] J. J. Yeh and I. Lindau, At. Data Nucl. Data Tables **32**, 1 (1985).

[42] M. B. Trzhaskovskaya and V. G. Yarzhemsky, At. Data Nucl. Data Tables **119**, 99 (2018).

[43] D. Takegami, L. Nicolaï, T. C. Koethe, D. Kasinathan, C. Y. Kuo, Y. F. Liao, K. D. Tsuei, G. Panaccione, F. Offi, G. Monaco, N. B. Brookes, J. Minár, and L. H. Tjeng, Phys. Rev. B **99**, 165101 (2019).

[44] S. Danzenbächer, D. V. Vyalikh, Yu. Kucherenko, A. Kade, C. Laubschat, N. Caroca-Canales, C. Krellner, C. Geibel, A. V. Fedorov, D. S. Dessau, R. Follath, W. Eberhardt, and S. L. Molodtsov, Phys. Rev. Lett. **102**, 026403 (2009).